AGU PUBLICATIONS

Geophysical Research Letters

RESEARCH LETTER
10.1002/2015GL067529

Key Points:
- Evidence of shear thermal instability for intermediate depth earthquake
- Relation between mantle dynamic processes and earthquake occurrence
- Strong dynamic stress variation is observed during earthquake rupture

Supporting Information:
- Supporting Information S1
- Figure S1
- Figure S2
- Figure S3
- Figure S4
- Figure S1–S4 captions

Correspondence to:
P. Poli,
ppoli@mit.edu

Citation:
Poli, P., G. Prieto, E. Rivera, and S. Ruiz (2016), Earthquakes initiation and thermal shear instability in the Hindu Kush intermediate depth nest, *Geophys. Res. Lett.*, *43*, doi:10.1002/2015GL067529.

Received 21 DEC 2015
Accepted 1 FEB 2016
Accepted article online 4 FEB 2016

Earthquakes initiation and thermal shear instability in the Hindu Kush intermediate depth nest

Piero Poli[1,2], German Prieto[1,2], Efrain Rivera[1,2], and Sergio Ruiz[1,2]

[1]Massachusetts Institute of Technology, Cambridge, Massachusetts, USA, [2]Geophysics Department, Universidad de Chile, Santiago, Chile

Abstract Intermediate depth earthquakes often occur along subducting lithosphere, but despite their ubiquity the physical mechanism responsible for promoting brittle or brittle-like failure is not well constrained. Large concentrations of intermediate depth earthquakes have been found to be related to slab break-off, slab drip, and slab tears. The intermediate depth Hindu Kush nest is one of the most seismically active regions in the world and shows the correlation of a weak region associated with ongoing slab detachment process. Here we study relocated seismicity in the nest to constraint the geometry of the shear zone at the top of the detached slab. The analysis of the rupture process of the M_w 7.5 Afghanistan 2015 earthquake and other several well-recorded events over the past 25 years shows an initially slow, highly dissipative rupture, followed by a dramatic dynamic frictional stress reduction and corresponding large energy radiation. These properties are typical of thermal driven rupture processes. We infer that thermal shear instabilities are a leading mechanism for the generation of intermediated-depth earthquakes especially in presence of weak zone subjected to large strain accumulation, due to ongoing detachment process.

1. Introduction

Three main mechanisms have been proposed as candidates responsible for high-pressure fracture [*Frohlich*, 1989; *Green and Houston*, 1995; *Kirby et al*., 1991; *Jung et al*., 2004; *Kelemen and Hirth*, 2007]. Dehydration embrittlement provides a significant change in pore pressure, thus decreasing the effect of normal stress, trough metamorphic dehydration reactions [*Jung et al*., 2004]. A second candidate is the faulting due to mineral phase transformation [*Kirby et al*., 1991]. Both these mechanisms are well documented from laboratory experience in crystalline materials [*Jung et al*., 2004; *Schubnel et al*., 2013]. The third mechanism is thermal shear instabilities [*John et al*., 2009] in which a strain temperature positive feedback reduces the friction and thus favoring brittle like rupture [*John et al*., 2009]. The latter is preferentially developed in preexisting shear zone, where localized creep plays the role of increasing the temperature [*Golding et al*., 2012; *Thielmann et al*., 2015] and lower the grain size [*Golding et al*., 2012] favoring ruptures at relatively low stress drop values (~10 MPa) [*Thielmann et al*., 2015].

On 26 October 2015 09:09:32 (UTC) a magnitude (M_w) 7.5 earthquake ruptured at 192.1 km depth within the Hindu Kush (HK) nest [*Prieto et al*., 2012] at the border between Afghanistan and Pakistan (Figure 1). This event is of main interest for several reasons. First, it occurs on the upper southern border of the Hindu Kush nest. Previous studies interpreted the discontinuous character of the seismicity in the area as due to a slab detachment process [*Sperner et al*., 2001; *Sippl et al*., 2013], with the HK nest being necked at its top, with a shear zone dipping toward the south [*Lister et al*., 2008]. The relocated hypocenter and aftershocks of the M_w 7.5 earthquake match the interpreted shear band at the top of the detached slab. Second, the earthquake is characterized by two completely different rupture stages (Figures 2 and S1 in the supporting information), stage 1: a ~ 10 s sub event with small *P* wave amplitude similar to a nucleation phase [*Ellsworth and Beroza*, 1995], followed by stage 2: a large *P* wave onset. Third, the M_w 7.5 event is the third M_w 7+ event occurring over the last 20 years in the nest. A two-stage rupture as observed for the M_w 7.5 event is also observed for each of the previous M_w 7+ earthquakes (Figure 3).

We here present a detailed study of both the geometry and the dynamic rupture process of the M_w 7.5 Afghanistan 2015 event, to get insights about the mechanism of intermediate depth faulting. We further analyze the previous seismicity to corroborate our hypothesis and gain insights about the long-term behavior of the seismicity in the area.

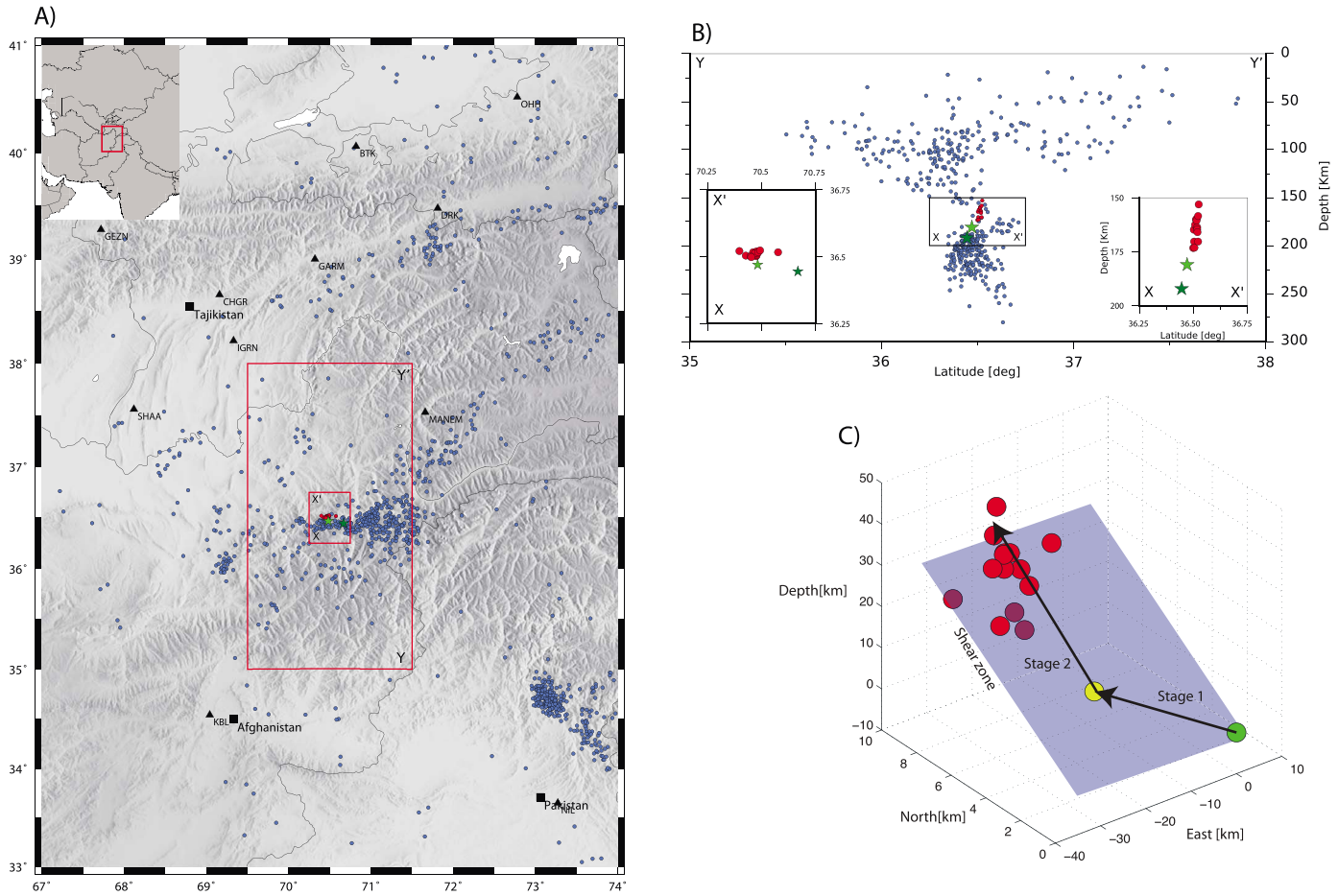

Figure 1. Location of the Hindu Kush nest. (a) Map of the studied region. Blue dots are the relocated seismic events [*Engdahl et al.*, 1998; EHB]. The dark and light green stars are hypocenter of the main event and of the large *P* wave onset, respectively. Red dots are the 14 relocated aftershocks. (b) The red boxes delimit the depth section. The depth distribution of the seismicity in the area is showed in Figure 1b. The relocated aftershocks clearly define a steeply south dipping plane at the top of the detached slab. We interpreted this plane as being a shear zone in which high strain rates are responsible of cyclic heating processing that trigger the occurrence of the seismic events. The two onsets are map and vertical section zoom for the main event and relocated aftershocks. (c) Summary of the magnitude 7.5 2015 earthquake. The rupture starts at the green dot, while the yellow dot represents the onset of the large amplitude *P* waves. After the large amplitude *P* wave onset the rupture has a main vertical component, as resolved by the relocated position by the aftershocks (red dots). The violet plane is the fault plane.

2. Analysis of Rupture Geometry

The M_w 7.5 event occurred on 26 October 2015 09:09:32 (UTC) is characterized by two rupture stages (Figure 2a). The arrival times from the *P* wave of stage 1 to the large *P* wave (stage 2) onset show clear rupture directivity (Figures 2a and S1), with the direction of shorter duration suggesting an eastward rupture. The duration of the small amplitude *P* wave event recorded at both regional and teleseismic stations can be used to quantitatively constrain the relative location of the large *P* wave onset.

We locate the hypocenter (stage 1), the large *P* wave onset (stage 2), and 14 aftershocks that occurred in the period between 26 October and 31 October 2015, with the NonLinLoc software [*Lomax et al.*, 2000] using a regional velocity model [*Sippl et al.*, 2013]. Our results show that the main energy burst starts 20 km east of the hypocenter, suggesting that stage 1 subevent occurs on a subhorizontal causative fault. The average estimated duration of stage 1 is ~10 s, for a rupture velocity (V_R) of 2 km/s, or V_R/V_S ~0.4 considering the local shear velocity (V_S) at the hypocenter depth [*Sippl et al.*, 2013]. After this first rupture stage, the rupture is characterized by large amplitude *P* waves lasting for about 25 s.

The hypocenter of the stage 1 is at focal depth of 192.1 km and is located at 34.4 N and 70.7 E (Figure 1), while the relocated aftershocks plotted in Figure 1 describe a narrow south dipping plane. The whole rupture is

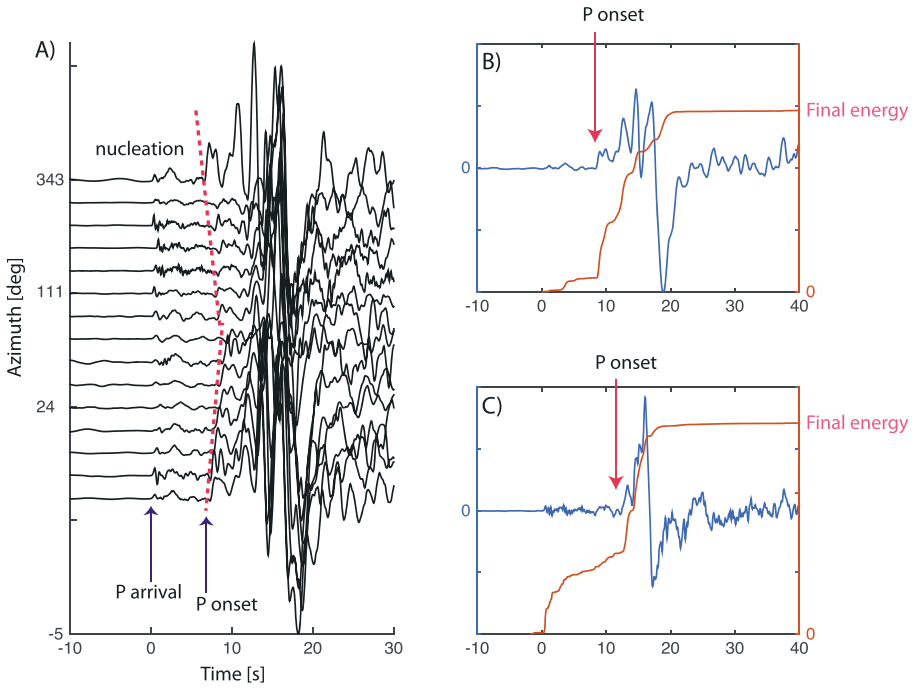

Figure 2. Analysis of seismic nucleation phase and dynamic energy release for the M_w 7.5 event. (a) Recorded seismograms as function of azimuth. The time zero corresponds to the handpicked *P* wave arrival. A clear low amplitude signals with variable azimuthal duration is visible. The red dashed lines delimit the beginning of large amplitude *P* waves. The velocity seismograms (blue) in Figures 2b and 2c are representative of the rupture processes. The red lines are the cumulative energy release as a function of rupture time. At the large *P* wave onset indicated by the red arrows the amount of energy released drastically increases, suggesting a variation of the frictional stress level during the rupture process.

taking place at the southern limit of the nest and is characterized by drastic change in rupture direction (Figure 1c), similar to proposed models for the Sea of Okhokts earthquake [*Chen et al*., 2014].

3. Earthquake Energy Balance

The two-stage rupture of the M_w 7.5 earthquake (Figures 2 and S1) suggests a change in the dynamic behavior of the rupture process. We used the picks of the low amplitude *P* waves to isolate the first part of the rupture (Figures 2 and S1). We then calculate the squared velocity spectra for each station, correct them for attenuation and focal mechanism [*Boatwright and Choy*, 1986], and estimate the radiated seismic energy (supporting information). The same processing is applied to the second part of the rupture up to 30 s after the onset of the large *P* waves amplitude (Figure 2). With the same relative parts of the signals we estimated the seismic moment for the two events.

The seismic moment of the first event is 8e18Nm while for the second stage is 1.e20Nm. The moment of the first part of the rupture is thus only 4% of the total moment release. The estimated energy release is 8.1e + 13 J and 9.4e + 15 J, respectively. The scaled energy (E/Mo, ratio of the seismic moment to the radiated energy) can be used to infer the dynamics of the rupture process [*Kanamori and Heaton*, 2000] and in this case we compare the results for the two stages of the earthquake. For stage 1 E/Mo = 1e-5, a value that is significantly smaller than typical crustal earthquakes [e.g., *Ide and Beroza*, 2001], suggesting a dissipative process during this stage. In stage 2, E/Mo = 9.4e-5, a value that is closer to that of crustal events [e.g., *Ide and Beroza*, 2001]. The temporal evolution of the rupture process is summarized in Figures 2b and 2c, where the velocity seismogram and the cumulative radiated energy are plotted for selected stations. The radical variation of *P* wave amplitude together with relative scaled energy suggests a dynamic change of the stress release. For example, a reduction of the dynamic frictional stress can explain the increase radiated energy during the slip process as discussed in *Kanamori and Heaton* [2000] and observed in laboratory experiment [*Di Toro et al*., 2006]. The overall rupture is similar to the one of the deep 1994 Bolivia earthquake (Figure S2) for which a frictional melting process

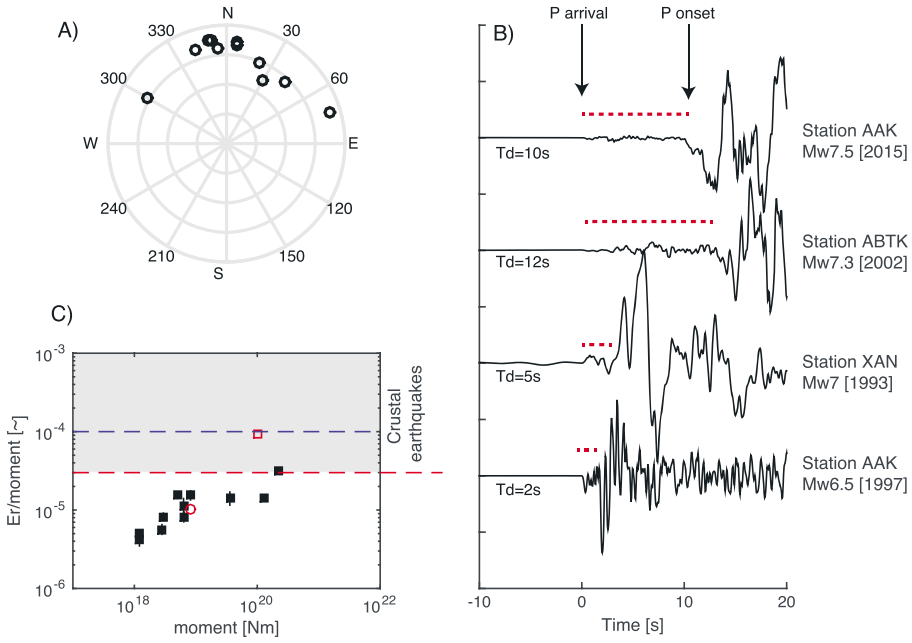

Figure 3. Geometry and energy balance for $M_w > 6$ earthquakes on the Hindu Kush nest. (a) Fault plane poles for the selected events. These poles describe a southward steeply dipping region similar to the shear zone discussed in *Lister et al.* [2008]. (b) Nucleation phases observed for a variety of events on the nest. Station, magnitude (M_w), and year of the event are reported next to each seismogram. (c) Scaled energy for the analyzed events. The value of scaled energy clearly increases with the size of the earthquakes. The red square is the estimated E_R/M_0 ratio for the second part of the main event, while the red dots are for the first part. The large difference between these two values suggests a strong variation of stress level during the rupture. The red and blue dashed lines represent the lower limit and the average of the scaled energy observed for earthquakes occurring at lower normal pressure (e.g., in crust).

has been constrained from seismological data [*Kanamori et al.*, 1998]. The Bolivia earthquake is characterized by an approximately 10 s (Figure S2) nucleation phase propagating for 20 km and releasing only 5% [*Kikuchi and Kanamori*, 1994] of the total moment and by low energy radiation [*Kanamori et al.*, 1998].

4. Analysis of Previous Seismicity

We additionally analyze nine earthquakes occurring in the HK nest from 1990 to 2015 to corroborate our hypothesis. These events are selected because of their location near the fault plane of the M_w 7.5 main event, and their focal mechanism is similar, suggesting their correlation with the shear zone (see Figures 3a and S3). For each event we estimate the radiated seismic energy (see supporting information). The scaled energy shown in Figure 3c illustrates how these events are less efficient than crustal earthquakes [*Ide and Beroza*, 2001]. The scaled energy increases as function of moment suggesting a scale-dependent rupture behavior. Additional dynamic weakening [*Di Toro et al.*, 2006] is more likely for large slip and larger events are prone to experience a drastic reduction of friction and give rise to the second, more energetic, rupture stage as in the M_w 7.5 earthquake studied here. The variation of scaled energy can be interpreted as increment in weakening distance for different size of events [*Cocco et al.*, 2009]. This hypothesis is corroborated by the observation of slow nucleation phases [*Ellsworth and Beroza*, 1995]. Out of the nine events, 4 $M_w > 6.5$ (including the 2015 Afghanistan earthquake) have a slow initial nucleation phase as illustrated in Figure 3b. The length of the nucleation is magnitude dependent and qualitatively fit the magnitude dependence of scaled energy (Figures 3b and S4).

5. Discussion

The resolved rupture geometry of the M_w 7.5 event in the HK nest confirms the idea of a shear zone localized at the southern border of the nest, as previously observed by *Lister et al.* [2008]. Our further constraint provided by the determination of the causative fault plane has wide implication in the context of debating the slab

detachment process in the area and its relation with orogeny evolution [*Lister et al*., 2008]. The resolved shear band has the same geometrical characteristics as observed in numerical modeling of slab detaching processes [*Duretz et al*., 2011]. Numerical simulations [*Duretz et al*., 2011] show that this shear zones are characterized by high-localized strain and are likely to undergo periodic episodes of significant shear heating [*Kelemen and Hirth*, 2007]. Given the strain accumulation, frictional stresses rapidly drop, generating earthquake radiation [*Kelemen and Hirth*, 2007; *Andersen et al*., 2008; *Thielmann et al*., 2015] even at relatively low stress values in presence of hydrous minerals [*Chernak and Hirth*, 2011] and small-grained rheology [*Thielmann et al*., 2015; *Chernak and Hirth*, 2011].

The rupture of the M_w 7.5 event is characterized by a strong change in dynamic stresses. The low energy to moment ratio in stage 1 suggests a low energy dynamically radiated as seismic waves [*Kanamori and Heaton*, 2000] during this first part of the event. The energy is thus dissipated on the fault region as friction and heating. The stage 1 of the rupture is likely to be the culmination of a shear-heating period [*Kelemen and Hirth*, 2007; *Deseta et al*., 2014; *Thielmann et al*., 2015].

Our preferred interpretation is that the M_w 7.5 event in the HK nest is due to thermal shear instability. This is not the only possible mechanism for generation of intermediate depth event, but our geometrical constraints, together with the results of *Lister et al*. [2008] plus the evidence of dynamic variation of stress levels, point toward this mechanism as a cause.

Previous events on the shear zone suggest highly dissipative rupture processes in general. The initiation of the largest events is characterized by a small nucleation phase followed by large energy release. This information together with the scaling of the energy to moment ratio implies significant dynamic stress changes during active rupture propagation [*Kanamori and Heaton*, 2000] with larger releasing having larger scaled energy after reduction of the dynamic frictional stress due to slip induced heating and melting [*Di Toro et al*., 2006]. We conclude that shear heating instabilities are responsible for the propagation of intermediate depth earthquake rupture, in particular along highly clustered seismicity regions.

Acknowledgments
The facilities of IRIS Data Services, and specifically the IRIS Data Management Center, were used for access to waveforms, related metadata, and/or derived products used in this study. IRIS Data Services are funded through the Seismological Facilities for the Advancement of Geoscience and EarthScope (SAGE) Proposal of the National Science Foundation under Cooperative Agreement EAR-1261681. The comments from Torgeir Andersen helped to improve the manuscript.

References

Andersen, T. B., K. Mair, H. Austrheim, Y. Y. Podladchikov, and J. C. Vrijmoed (2008), Stress release in exhumed intermediate and deep earthquakes determined from ultramafic pseudotachylyte, *Geology*, *36*(12), 995–998.

Boatwright, J., and G. L. Choy (1986), Teleseismic estimates of the energy radiated by shallow earthquakes, *J. Geophys. Res.*, *91*(B2), 2095–2112, doi:10.1029/JB091iB02p02095.

Chen, Y., L. Wen, and C. Ji (2014), A cascading failure during the 24 May 2013 great Okhotsk deep earthquake, *J. Geophys. Res. Solid Earth*, *119*, 3035–3049, doi:10.1002/2013JB010926.

Chernak, L. J., and G. Hirth (2011), Syndeformational antigorite dehydration produces stable fault slip, *Geology*, *39*(9), 847–850.

Cocco, M., E. Tinti, C. Marone, and A. Piatanesi (2009), Scaling of slip weakening distance with final slip during dynamic earthquake rupture, *Int. Geophys.*, *94*, 163–186.

Deseta, N., L. D. Ashwal, and T. B. Andersen (2014), Initiating intermediate-depth earthquakes: Insights from a HP–LT ophiolite from Corsica, *Lithos*, *206*, 127–146.

Di Toro, G., H. Takehiro, S. Nielsen, G. Pennacchioni, and T. Shimamoto (2006), Natural and experimental evidence of melt lubrication of faults during earthquakes, *Science*, *311*(5761), 647–649.

Duretz, T., T. V. Gerya, and D. A. May (2011), Numerical modelling of spontaneous slab breakoff and subsequent topographic response, *Tectonophysics*, *502*(1), 244–256.

Ellsworth, W. L., and G. C. Beroza (1995), Seismic evidence for an earthquake nucleation phase, *Science*, *268*(5212), 851.

Engdahl, E. R., R. van der Hilst, and R. Buland (1998), Global teleseismic earthquake relocation with improved travel times and procedures for depth determination, *Bull. Seismol. Soc. Am.*, *88*, 722–743.

Frohlich, C. (1989), The nature of deep-focus earthquakes, *Annu. Rev. Earth Planet. Sci.*, *17*, 227.

Golding, N., E. M. Schulson, and C. E. Renshaw (2012), Shear localization in ice: Mechanical response and microstructural evolution of P-faulting, *ActaMaterialia*, *60*(8), 3616–3631.

Green, H. W., and H. Houston (1995), The mechanics of deep earthquakes, *Annu. Rev. Earth Planet. Sci.*, *23*, 169–214.

Ide, S., and G. C. Beroza (2001), Does apparent stress vary with earthquake size?, *Geophys. Res. Lett.*, *28*(17), 3349–3352, doi:10.1029/2001GL013106.

John, T., S. Medvedev, L. H. Rüpke, T. B. Andersen, Y. Y. Podladchikov, and H. Austrheim (2009), Generation of intermediate-depth earthquakes by self-localizing thermal runaway, *Nat. Geosci.*, *2*(2), 137–140.

Jung, H., H. W. Green II, and L. F. Dobrzhinetskaya (2004), Intermediate-depth earthquake faulting by dehydration embrittlement with negative volume change, *Nature*, *428*(6982), 545–549.

Kanamori, H., and T. H. Heaton (2000), Microscopic and macroscopic physics of earthquakes, *Geophys. Monogr. AGU*, *120*, 147–164.

Kanamori, H., D. L. Anderson, and T. H. Heaton (1998), Frictional melting during the rupture of the 1994 Bolivian earthquake, *Science*, *279*(5352), 839–842.

Kelemen, P. B., and G. Hirth (2007), A periodic shear-heating mechanism for intermediate-depth earthquakes in the mantle, *Nature*, *446*(7137), 787–790.

Kikuchi, M., and H. Kanamori (1994), The mechanism of the deep Bolivia earthquake of June 9, 1994, *Geophys. Rese. Lett.*, *21*(22), 2341–2344, doi:10.1029/94GL02483.

Kirby, S. H., W. B. Durham, and L. A. Stern (1991), Mantle phase changes and deep-earthquake faulting in subducting lithosphere, *Science*, *252*(5003), 216–225.

Lister, G., B. Kennett, S. Richards, and M. Forster (2008), Boudinage of a stretching slablet implicated in earthquakes beneath the Hindu Kush, *Nat. Geosci.*, *1*(3), 196–201.

Lomax A., Virieux J., Volant P., Berge-Thierry C. (2000), Probabilistic earthquake location in 3D and layered models, in *Advances in Seismic Event Location*, pp. 101–134, Springer, Netherlands, doi:10.1007/978-94-015-9536-0_5.

Prieto, G. A., G. C. Berozab, S. A. Barrettb, G. A. López c, and M. Floreza (2012), Earthquake nests as natural laboratories for the study of intermediate-depth earthquake mechanics, *Tectonophysics*, *570*, 42–56.

Schubnel, A., F. Brunet, N. Hilairet, J. Gasc, Y. Wang, and H. W. Green II (2013), Deep-focus earthquake analogs recorded at high pressure and temperature in the laboratory, *Science*, *341*(6152), 1377–1380.

Sippl, C., et al. (2013), Geometry of the Pamir-Hindu Kush intermediate-depth earthquake zone from local seismic data, *J. Geophys. Res. Solid Earth*, *118*, 1438–1457, doi:10.1002/jgrb.50128.

Sperner, B., F. Lorenz, K. Bonjer, S. Hettel, B. Müller, and F. Wenzel (2001), Slab break-off–abrupt cut or gradual detachment? New insights from the Vrancea Region (SE Carpathians, Romania), *Terra Nova*, *13*(3), 172–179.

Thielmann, M., A. Rozel, B. J. P. Kaus, and Y. Ricard (2015), Intermediate-depth earthquake generation and shear zone formation caused by grain size reduction and shear heating, *Geology*, *43*(9), 791–794.